Ab initio study of ferroelectric domain walls in $PbTiO_3$

B. Meyer and David Vanderbilt
Department of Physics and Astronomy,
Rutgers University, Piscataway, New Jersey 08854-8019, USA
(September 13, 2001)

We have investigated the atomistic structure of the 180° and 90° domain boundaries in the ferroelectric perovskite compound $PbTiO_3$ using a first-principles ultrasoft-pseudopotential approach. For each case we have computed the position, thickness and creation energy of the domain walls, and an estimate of the barrier height for their motion has been obtained. We find both kinds of domain walls to be very narrow with a similar width on the order of one to two lattice constants. The energy of the 90° domain wall is calculated to be $35\,\mathrm{mJ/m^2}$, about a factor of four lower than the energy of its 180° counterpart, and only a miniscule barrier for its motion is found. As a surprising feature we detected a small offset of 0.15–0.2 eV in the electrostatic potential across the 90° domain wall.

PACS numbers: 77.80.Dj, 77.84.Dy, 61.72.Mm, 68.35.Ct

I. INTRODUCTION

After cooling below the transition temperature, ferroelectric crystals usually adopt a very complex microstructure consisting of regions with different orientations of the spontaneous polarization. These domains are formed to reduce uncompensated depolarization fields at the surface, releasing elastic strain and so lowering the free energy of the crystal. The domain structure and the properties of the domain boundaries play an important role in the performance of many ferroelectric devices. Mechanical and electrical characteristics, such as the permittivity, coercive field, and piezoelectric constants, are often significantly influenced. In particular, the thickness and the interfacial energy of the domain walls are important parameters in understanding the switching kinetics and fatigue mechanism in ferroelectric materials. The width affects the wall mobility, and the energy determines how easily new domain walls may be introduced during polarization reversal processes. Thus, for a thorough understanding of the physical processes associated with the switching and fatigue behavior of a ferroelectric material, an accurate microscopic description of the underlying domain walls and their dynamics is required.

A phenomenological level of description has been used in most previous theoretical investigations of ferroelectric domain walls. Several authors have modeled the structure of domain walls by using a Landau-Ginzburg type of continuum theory.[1–3] The domain wall is described by a soliton solution, giving the polarization profile and the distribution of the elastic strain across the domain wall, from which the domain wall width and energy can be deduced. For example, in a very early work Zhirnov[1] obtained estimates for the thickness of domain walls in $BaTiO_3$. He found the 180° domain wall to be atomically sharp with a width of only 5–20 Å, but he predicted the 90° domain wall to be much broader with a thickness of 50–100 Å. This different picture of 180° and 90° domain walls has been quite commonly accepted since then.[4] However, some of the parameters needed in the expansion of the free energy functional can only roughly be estimated from the experimental data available, the empirical approaches based on Landau-Ginzburg theory are rather limited and tend to be more qualitative in nature. Also, for atomically sharp domain walls the applicability of continuum theoretical models is questionable. Thus, for a deeper theoretical understanding of domain walls, more accurate atomistic calculations are need.

A first work in this direction was undertaken by Padilla, Zhong, and Vanderbilt[5] who investigated 180° domain walls in tetragonal $BaTiO_3$ using an effective Hamiltonian derived from first-principles calculations. With this effective Hamiltonian, Monte-Carlo simulations at finite temperatures were performed to calculate the energy, free energy and thickness of the wall. A very narrow domain wall with energy $16\,\mathrm{mJ/m^2}$ was found.

With a first-principles pseudopotential method based on density-functional theory, Pöykkö and Chadi[6] studied the 180° domain wall in $PbTiO_3$. They confirmed a picture in which 180° walls are very narrow, but found a much higher domain-wall energy than for $BaTiO_3$.

In this paper, we undertake a first-principles study of the 180° and 90° domain walls in $PbTiO_3$. For both domain wall types we have calculated the fully relaxed atomic structure, the domain-wall energy, the polarization profile across the domain wall, and an estimate of the barrier height for their motion. As for the 180° domain wall, our study is similar in spirit to the work of Pöykkö and Chadi, but the conclusions differ in some important respects. However, the main focus of this paper will be on the 90° domain wall, where we are not aware of any previous first-principles study for a ferroelectric perovskite. The 90° domain wall is of particular interest because some detailed experimental results on its atomistic structure have recently become available. (The experimental investigation of the 180° domain wall is much more difficult.) Some of the experiments on the 90° domain wall have created considerable doubt regarding the commonly accepted picture that the 90° domain wall is much broader than its 180° counterpart. With the present simultaneous study of the 90° and 180° domain wall, we provide strong support, at least in the case of defect-free walls at low temperature, that both domain walls are of comparable width. However, we find that the barrier for the motion of the 90° domain wall is extremely small, suggesting that at non-zero temperatures the domain walls may fluctuate strongly.

Many experimental techniques are capable of revealing the domain microstructure of a ferroelectric crystal,[4] but it is much more difficult to image the domain boundaries and determine their structure with atomic-level accuracy. Most studies so far have used high-resolution transmission electron microscopy (HRTEM) to obtain direct images of the domain walls.[7–11] In a detailed study of 90° domain walls in $BaTiO_3$ and $Pb(Zr_{0.52}Ti_{0.48})O_3$ Tsai et al.[8] observed a diffuse dark contrast about 4–10 unit cells wide in their HRTEM images of domain boundaries, which they attributed to deviations from the Bragg condition through lattice distortions and ionic displacements. But no further analysis of these images was done. Combining HRTEM and quantitative image analysis, Stemmer et al.[9] measured the width of the 90° domain wall in $PbTiO_3$ to be 10 ± 3 Å, and they gave an estimate for the domain-wall energy of $50\,\mathrm{mJ/m^2}$. This evidence for a very narrow 90° domain wall in $PbTiO_3$ was further confirmed by Foeth et al.[11] From their HRTEM images they obtained a width of 15 ± 3 Å at room temperature, and from the analysis of the thickness fringes of weak-beam transmission electron microscopy (WBTEM) they found a value of 21 ± 7 Å. In contrast, Floquet et al.[11] concluded, based on their combined study of HRTEM images and a careful analysis of the X-ray diffraction pattern (XRPD) of $BaTiO_3$, that 90° domain walls are regions of width 40–60 Å where the crystallographic discontinuity is accommodated by irregular atomic displacements. For micron-sized $BaTiO_3$ grains they even proposed a wall thickness of 140 Å.

This paper is organized as follows. In Section II we describe the technical details of our computational method and the geometry of the supercells used to model the domain walls. In Section III and IV we present our results on the 180° and 90° domain walls, respectively. Finally, the paper concludes with a summary, Section V, in which we also discuss the results in the context of the previous experimental work.

II. THEORETICAL DETAILS

A. Method of calculation

For our calculations we have used a first-principles plane-wave pseudopotential method based on density-functional theory (DFT)[12] within the local-density approximation (LDA).[13] Ab-initio simulations of this kind have be applied successfully many times to explain the origin of ferroelectricity in perovskite compounds,[14] to determine ground-state structures[15] and to reproduce sequences of phase transitions.[16] The spontaneous polarization,[17] Born effective charges,[18,19] piezoelectric coefficients[20] and other material parameters[21] have been calculated in excellent agreement with experiment. Also defects[22] and surfaces[23,24] in ferroelectric materials have been studied using DFT methods.

	Theory	Exp.[a]
a [Å]	3.86	3.90
c [Å]	4.04	4.15
ξ_z(Pb)	0.71	0.72
ξ_z(Ti)	0.34	0.33
$\xi_z(\mathrm{O_I})$	−0.39	−0.35
$\xi_z(\mathrm{O_{II}})$	−0.39	−0.35
$\xi_z(\mathrm{O_{III}})$	−0.27	−0.35
$\lvert\xi\rvert$ [Å]	0.38	0.43

TABLE I. Computed and experimental values of the structural parameters for bulk $PbTiO_3$ in the tetragonal phase. a and c are the lattice constants, and the atomic displacements relative to the cubic positions are given as a unit vector $\hat{\xi}$ times an amplitude $|\xi|$. For the labels of the oxygen atoms see Fig. 1(a).

[a] Ref. 26.

The pseudopotentials were of the Vanderbilt ultrasoft type[25] with the semicore Pb $5d$ and Ti $3s$ and $3p$ states explicitly treated as valence states (in contrast to Ref. 6). A conjugate gradient technique as described in Ref. 15 was employed to minimize the Hohenberg-Kohn total energy functional. For the plane-wave expansion of the electron wavefunctions a cutoff energy of 25 Ry was used. The same pseudopotentials have already been used in several previous studies on $PbTiO_3$ where their accuracy has been demonstrated,[15,24] and where it has been shown that a cutoff energy of 25 Ry is sufficient to obtain very well converged results. The resulting computed structural parameters for the tetragonal phase of $PbTiO_3$ are given in Table I. The lattice constants a and c are underestimated by 1 % and 2.6 %, respectively, which is typical for LDA. The deviations in the atomic displacements of the oxygen ions between theory and experiment are mainly due to the fact that the X-ray data were analyzed under the assumption that the displacement is the same for all three oxygen atoms.

The construction of appropriate supercells for the study of the domain walls of interest will be detailed in the following subsection. All atomic configurations were fully relaxed by minimizing the atomic forces using a variable-metric scheme.[27] Convergence was assumed when the forces on the ions were less than $0.005\,\mathrm{eV/Å}$.

B. Domain wall geometries

$PbTiO_3$ belongs to the important group of ferroelectric materials based on the cubic perovskite structure. At the temperature of 765 K $PbTiO_3$ undergoes a single phase transition from the paraelectric cubic phase to a tetragonally distorted ferroelectric phase, Fig. 1(a), and remains in this tetragonal phase down to $T = 0$. In this state, six energetically equivalent orientations of the spontaneous polarization exist. The domain walls between these variants can be regarded as twin boundaries on low-index lattice planes. With the additional constraint that the normal component of the polarization should be continuous across the domain wall, so that no net interface charge is present, there are two allowed types: (i) twins on (100) planes with parallel polarization of opposite orientation in the neighboring domains (180° domain wall); and (ii) twins on (101) planes with the polarizations on either side of the domain wall being almost perpendicular to one another (90° domain wall). These situations are illustrated in Figs. 1(b) and (c), respectively.

For 180° domain walls, two possible high-symmetry cases exist. These are Pb–centered and Ti–centered domain walls, resulting from twinning on PbO– and TiO_2–planes, respectively. In each case one of the metal cations acts as a center of inversion symmetry. Of course, we have to check whether one of these symmetries is actually present, or whether the atomic relaxation leads to a lower-symmetry structure; we will return to this point in Sec. III.

For the 90° domain wall, we can imagine obtaining a starting structure by twinning on either Pb–Ti–O or O–O types of (101) planes. However, in this case the "flow" of the polarization establishes an intrinsic difference between the "upstream" and "downstream" sides of the domain wall (left and right sides, respectively, in Fig. 1(c)). Thus, the two sides of the domain wall cannot be related by any symmetry operation, and there is no possible scenario in which the position of the domain wall is determined by symmetry. In other words, we expect that if we start from either starting guess, the structure will relax to some ground-state structure located at some intermediate position between the Pb–Ti–O and O–O limits. There is thus no sharp distinction between a Pb–Ti–O or an O–O centered domain wall in the 90° case. In our calculations, we start the relaxation from the structure obtained by twinning on the Ti–Pb–O plane. (As we shall see, the relaxed structure ends up being centered much closer to the O–O plane, so clearly we introduce no bias by doing so.)

Since periodic boundary conditions are used in plane-wave pseudopotential calculations, we cannot study single domain walls in isolation. Instead we have to build supercells containing a domain structure that can be repeated periodically in three dimensions. As a consequence, we always have to include two domain walls in a supercell.

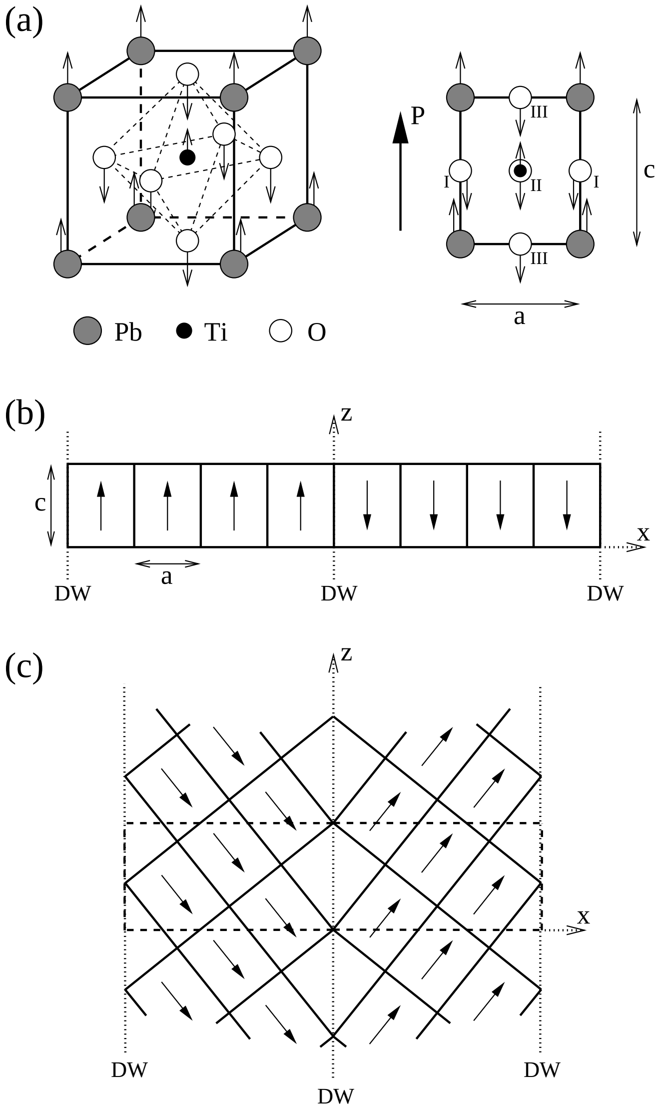

FIG. 1. (a) Unit cell of the cubic perovskite structure and its projection along the [010] direction; arrows indicate atomic displacements in the ferroelectric tetragonal phase. (b–c) Supercell geometries containing 8 perovskite primitive cells for (b) 180° and (c) 90° domain walls (DW's); atoms are omitted and only solid lines connecting the Pb atoms are drawn. Supercell boundaries are indicated by dashed lines.

For the simulation of the 180° domain wall, we have used supercells consisting of $N \times 1 \times 1$ perovskite unit cells stacked in the x direction and containing one "up" and one "down" domain, each $N/2$ lattice constants wide, as shown in Fig. 1(b). We take the domain wall to lie in the y–z plane and the polarization to point in the z–direction. Supercells with $N = 6$, 8 and 10 were employed, containing 30, 40 and 50 atoms, respectively. The dimensions of the supercell were kept fixed at the theoretical equilibrium lattice constants computed for the bulk tetragonal phase (see Table I). For all Brillouin-zone integrations a (2,4,4) Monkhorst-Pack k-point mesh[28] was used; this k–point mesh has previously been shown to be sufficient for $PbTiO_3$.[24]

The geometry of the supercell containing two 90° domain walls is sketched in Fig. 1(c). The tetragonal shape of the $PbTiO_3$ unit cell causes the angle between the c axes on either side of the domain wall to deviate slightly from 90°. Instead, to form a coherent twin interface, an angle of $2\arctan(a/c)$ is geometrically required. This gives rise to a very characteristic bending of the [100] and [001] atomic rows (a– and c–rows) across the domain wall; in fact, this bending is precisely the signature through which 90° domain walls are identified in HRTEM images.[9] Again, we have taken the domain wall to lie in the y–z plane and the x direction to be perpendicular to the wall. The supercell is orthorhombic with dimensions of $Nc/\sqrt{1+(c/a)^2}$, a, and $a\sqrt{1+(c/a)^2}$ in the x–, y–, and z–directions, respectively. We used supercells consisting of N= 6, 8, 10, 12 and 14 perovskite unit cells, thus containing up to 70 atoms. The theoretical LDA values from Table I were taken for the lattice parameters a and c. For one supercell we also relaxed the lattice constant in the x direction, but the resulting expansion of the supercell in the x direction was very small (less than 0.8 % of a), and the changes in the atomic displacements and in the domain-wall energy were negligible. Two symmetry operations were imposed during the atomic relaxation: a mirror operation across the y=0 plane, and a glide mirror operation across the z=0 plane with a translation of half the superlattice dimension in the x direction. The first symmetry corresponds to a physical assumption that the polarization does not rotate out of the y=0 plane, while the second is just a technical convenience to insure that both domains in the supercell stay equivalent. For the Brillouin zone sampling again a (2,4,4) Monkhorst-Pack k–point mesh[28] was used.

III. RESULTS FOR THE 180° DOMAIN WALL

We have investigated both the Pb– and Ti–centered domain walls. The relaxation of the atomic structure was started from the ideal twinned configurations, and the inversion symmetry centered on a cation in the domain wall was enforced during the structural optimization process. This prevents a Ti–centered domain wall from transforming into a Pb–centered wall or vice versa.

A. Domain wall energy

The results for the domain-wall energies from our various supercells are summarized in Table II. The reference energy of the bulk structure (without domain walls) was calculated from a single perovskite unit cell using a k–point mesh equivalent to the one used for the supercell. Values for $BaTiO_3$ are given for comparison; these were calculated by the same procedure except that a (2,6,6) k–point mesh was employed.

	$PbTiO_3$		$BaTiO_3$	
N	Pb–centered	Ti–centered	Ba–centered	Ti–centered
6	132	169	7.2	16.5
8	132	169	7.4	16.7
10	132	169	7.5	16.8

TABLE II. Calculated 180° domain-wall energies (mJ/m^2) using supercells of N perovskite primitive cells.

All relaxed structures have inversion symmetry about a cation in the domain wall (as well as mirror symmetry about the y=0 plane). The domain-wall energy is lowest for the Pb–centered domain wall; this is therefore the preferred wall configuration. The same ordering holds for $BaTiO_3$, but the domain-wall energies are significantly lower. As can be seen from the Table, the domain-wall energy is well converged even with the smallest separations of the domain walls.

In contrast, Pöykkö and Chadi[6] found that domains have to be at least four lattice constants wide before the up/down domain pattern becomes stable. Furthermore, their calculations indicated that the Pb–centered domain-wall energy could be lowered by almost a factor of two by breaking the inversion symmetry about a Pb atom in the domain wall. In their lowest-energy structure, in which there are large relaxations of Pb and O positions in the domain-wall plane, the only remaining symmetry was a 180° rotation about a z–axis (C_{2z}) passing through the center of a domain. In view of those results, we made careful tests in which we lowered the symmetry of our supercell in two ways: (i) as in the final result of Ref. 6, we kept only the C_{2z} symmetry about the center of a domain; and (ii) as in the case of the 90° domain wall, we kept only the glide mirror plane at z=0 with a half-supercell translation along x. We then distorted the atomic configuration in several ways compatible with the lowered symmetry and started a new atomic relaxation. In all cases, the structure relaxed back toward the high-symmetry centrosymmetric structure. The relaxation is very slow, indicating a very flat energy surface, but we never found a lower-energy structure with reduced symmetry.

Regarding the domain-wall energy, our value of 132 mJ/m^2 for the Pb–centered wall is much lower than the value of 270 mJ/m^2 obtained in Ref. 6 when inversion symmetry is imposed. Strangely, it is much closer to the 150 mJ/m^2 value reported in Ref. 6 when inversion symmetry breaking is allowed. For the Ti–centered domain wall our wall energy of 169 mJ/m^2 again lies below their value of 220 mJ/m^2. The case of a Ti–centered wall with broken inversion symmetry cannot be considered, since relaxation of the domain wall would then just transform it into a Pb–centered wall, as we will show in Sec. III C.

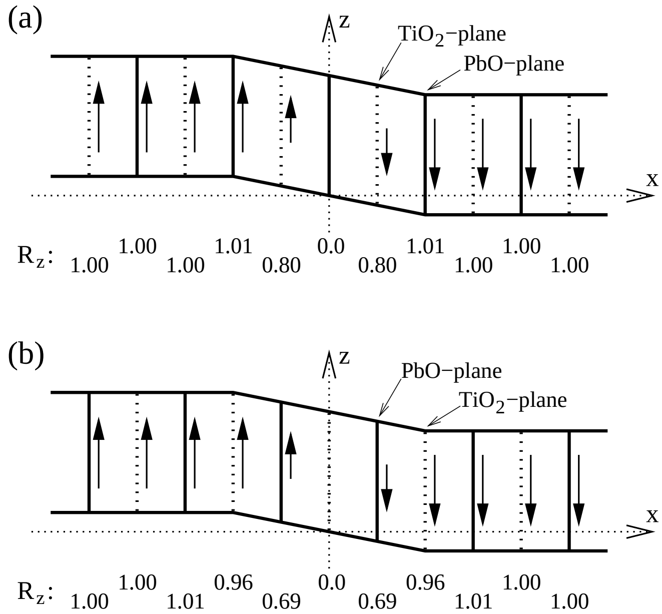

FIG. 2. Change of polarization across the (a) Pb–centered, and (b) Ti–centered, 180° domain wall. R_z denotes the ferroelectric distortion of each lattice plane in the z direction, in units of the distortion associated with the bulk spontaneous polarization.

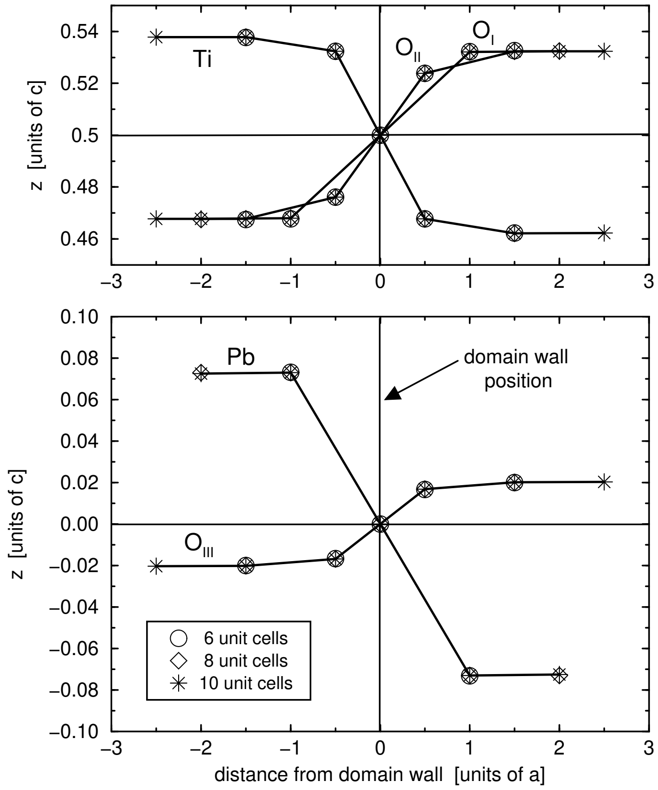

FIG. 3. The z–displacement of the atoms relative to the Pb atom in a Pb–centered 180° domain wall as function of the distance to the wall, calculated with different supercell sizes N. Integer distances represent PbO planes, half-integer distances TiO_2 planes. Labels of oxygen atoms correspond to those in Fig. 1(a).

B. Atomistic domain wall structure

We begin by analyzing how much the ferroelectric distortions along the z direction are changed by the presence of a domain wall. To give a quantitative description we compute an average ferroelectric distortion $\delta_{\rm FE}$ for each atomic plane parallel to the domain wall. As a measure for $\delta_{\rm FE}$ we take the displacement of the metal atom relative to an oxygen atom in the PbO or TiO_2 plane.[23,24] (In the case of a TiO_2 plane, we choose the oxygen ion lying along the z direction from the Ti atom.) We then define the parameter R_z as the ratio between $\delta_{\rm FE}$ of the specified lattice plane and its value in the undistorted ferroelectric bulk phase. R_z is a very sensitive indicator of the ferroelectric order: R_z is zero as long as the atoms are in their cubic positions, and tends to unity as the full bulk ferroelectric distortion is attained.

The results for the distortion R_z are illustrated in Fig. 2 for both Pb–centered and Ti–centered domain walls. Only the results from the 50-atom supercells are shown; results for smaller cells are essentially identical. We focus our discussion here on the more physical Pb–centered domain wall. We find that $R_z = 0.80$ already for the TiO_2 first-neighbor plane (to be compared with the value of 0.73 reported in Ref. 6), and the ferroelectric distortion is essentially fully recovered to its bulk value by the PbO second-layer plane. The orientation of the polarization thus changes abruptly over a distance of less than two lattice constants, leading to a very narrow domain wall. The narrowness of the 180° domain wall had earlier been predicted based on phenomenological models[1] and confirmed using atomic force microscopy (AFM).[29] The results for the Ti–centered wall are qualitatively similar.

In the next step we analyze for the Pb–centered domain wall how the atomic rows are aligned across the wall. As already indicated in Fig. 2, there is a considerable offset between [100] atomic rows to the left and right of the domain wall. Fig. 3 shows the detailed results for the z displacements of the atom rows relative to the Pb ion in the domain wall. The discontinuity in the [100] rows is largest for the Pb atoms, where we find a jump of 14.5 % of the lattice constant c. This offset of 0.6 Å should be clearly visible in an HRTEM image, thus allowing identification of 180° domain walls having polarization parallel to the surface in the neighboring domains.

It is not surprising that the largest offset occurs for the Pb rows, since the Pb displacement contributes most to the ferroelectric soft-mode vector (see Table I). By compensating for the different contributions of the atoms to the ferroelectric soft-mode vector, we can define a kind of "geometrical offset" between neighboring domains. We do this by going to the center of each domain and subtracting the bulk ferroelectric displacement pattern from

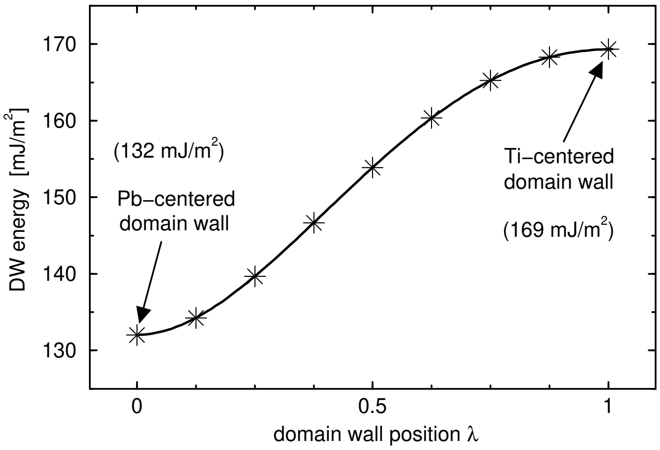

FIG. 4. Energy profile along the estimated path for the motion of a 180° domain wall, calculated with supercells of 10 perovskite unit cells.

the atomic coordinates, thereby shifting all atoms into essentially cubic positions. The offsets of the resulting atomic rows are now the same for all five atoms, and this joint offset therefore provides a reasonable measure of the geometrical misalignment. It turns out that this geometrical offset is very small; we found values of $0.010\,c$ and $0.008\,c$ for Pb–centered and Ti–centered walls respectively.

C. Barrier for domain wall motion

Many models have been proposed in the literature for the motion of domain walls in crystals. Most realistic models involve the formation and propagation of kinks of various shapes, allowing the domain wall to shift gradually to its new position. It is not our aim here to comment on or distinguish between these models; instead, we concentrate only on extracting one parameter that may be needed in many models of this type. Specifically, we compute the barrier height for coherent motion of the entire domain wall to its neighboring lattice position. Thus, our calculations always preserve full translational symmetry parallel to the domain wall.

We made a simple estimate for the path in configuration space along which a Pb–centered domain wall may gradually transform into a Ti–centered wall as follows. We took the atomic configurations $\xi_{\rm Pb}$ and $\xi_{\rm Ti}$ of Pb– and Ti–centered walls on neighboring lattice planes and formed the linear interpolation $\xi_{\rm Pb}+\lambda(\xi_{\rm Ti}-\xi_{\rm Pb})$, where λ has the interpretation of being a reaction coordinate along the path. The energy profile along this path is shown in Fig. 4. The configurations of the Pb– and Ti–centered domain wall are local minima and maxima of the energy curve, respectively, with no barrier between them. The Ti–centered wall is therefore metastable and will transform spontaneously into a Pb–centered domain wall. In our calculation the Ti–centered wall could only be stabilized by imposing a center of inversion symmetry in the domain wall. Moreover, Fig. 4 does not give any indication that the energy of the Pb–centered domain wall can be lowered by breaking the inversion symmetry. Having identified the Ti–centered domain wall as the saddle point configuration for the motion of a 180° domain wall, the barrier height for a jump to the nearest-neighbor lattice position is given by the difference between the wall energies of the Ti– and Pb–centered walls. We find this difference to be $37\,{\rm mJ/m^2}$.

N	6	8	10	12	14
$E_{\rm DW}$	29.4	32.5	34.6	34.7	35.2
$E_{\rm barrier}$	0.6	1.1	1.4	1.5	1.6

TABLE III. Calculated 90° domain-wall energies $E_{\rm DW}$ and barrier height for domain wall motion $E_{\rm barrier}$ $({\rm mJ/m^2})$ as function of supercell size N.

IV. RESULTS FOR THE 90° DOMAIN WALL

A. Domain wall energy

For an accurate calculation of the domain-wall energy, it is indispensable to reduce all effects of systematic errors as far as possible, since an uncertainty of only 10 meV in the energy difference between the supercell calculation and the reference structure already leads to an inaccuracy of $7.5\,{\rm mJ/m^2}$ in the domain-wall energy. Because of the particular shape of the supercells representing the 90° domain wall (as described in Sec. II B), it is not possible to construct equivalent k–point meshes for the supercells and single perovskite unit cells (in contrast to the 180° case). To get good energy differences between the relaxed structures and the bulk reference, we applied the following procedure for calculating the domain-wall energies. First, for the full atomic relaxation of the supercells, we used our regular (2,4,4) Monkhorst-Pack k–point mesh. Then, to reduce the k–point errors further, we reran the total-energy calculation of the supercell with a denser (2,6,6) Monkhorst-Pack mesh. The reference energy of the bulk structure was computed from a single perovskite unit cell using a k–point mesh with the same density and an orientation that corresponds as closely as possible to the supercell (2,6,6) Monkhorst-Pack mesh. Specifically, we employed a (N,6,6) Moreno-Soler k–point mesh[30] oriented along the [101], [010], and [$\bar{1}$01] directions (see Fig. 1(c)).

The results for the 90° domain-wall energies from the various supercells are given in Table III. The convergence of the wall energy with supercell size is somewhat slower than for the 180° case, but the energy is well converged for a wall separation of five perovskite unit cells. The calculated value of $35\,\mathrm{mJ/m^2}$ is in reasonable agreement with a rough estimate of $50\,\mathrm{mJ/m^2}$ from a HRTEM experiment.[9] The energy of the 90° domain wall is thus calculated to be about four times lower than that of its 180° counterpart, and we can conclude that the 90° domain wall is the most stable wall configuration in $PbTiO_3$.

B. Domain wall structure and polarization profile

In the case of the 180° domain wall the analysis of how the ferroelectric distortions change in the vicinity of the domain wall was relatively straightforward, since the question could be treated as a one-dimensional problem (the relaxation of the atoms in the x–direction, perpendicular to the domain wall, being completely negligible). In contrast, for the 90° domain wall the two-dimensional relaxations of the atoms lead to a complex relaxation pattern for which an analysis in terms of average ferroelectric distortions $\delta_{\rm FE}$ and their ratio relative to the bulk value R_z would be difficult to repeat.

Therefore, to simplify the discussion of the changes in the ferroelectric distortions, we have chosen to visualize the atomic displacements by translating them into a "polarization $\mathbf{P}^{(i)}$ per unit cell i" as follows. First, we have to decide what we mean by a "unit cell" in the context of the domain-wall structure. Figure 5 shows three possible ways of doing this. For the 'Ti-centered' choice, for example, the unit cell contains the central Ti atom, but the six neighboring O atoms are each shared by two unit cells, and the eight neighboring Pb atoms are each shared by eight unit cells. Thus we assign weights $w_{\rm Ti}$=1, $w_{\rm O}$=1/2, and $w_{\rm Pb}$=1/8 to describe the association of atoms to the unit cell. Two other choices are the 'Pb-centered' and 'M-centered' (metal-centered) cells, also illustrated in Fig. 5. The M-centered cell is the most compact in the x direction; it therefore gives the finest possible resolution to the function $\mathbf{P}(x)$ in the case of the 90° domain wall, which consists of alternate Pb–Ti–O– and O–O–type (101) planes stacked along x (see Fig. 1(c)). Next, we attach a polarization to each unit cell i via the assignment

$$\mathbf{P}^{(i)} = \frac{e}{\Omega_c} \sum_\alpha w_\alpha \, \mathbf{Z}^*_\alpha \cdot \mathbf{u}^{(i)}_\alpha \quad . \tag{1}$$

Here e is the electron charge, Ω_c the volume of the five-atom bulk unit cell, index α runs over all atoms of unit cell i, $\mathbf{u}^{(i)}_\alpha$ is the displacement of atom α from its cubic position, and w_α are the weight factors introduced above. The $\mathbf{Z}^*_\alpha$ are the Born effective charge tensors, which are approximated by their cubic bulk values as discussed below.

For the case of a homogeneous system having the primitive five-atom periodicity, Eq. (1) is independent of cell index i, and even of the choice of unit cell in Fig. 5; in

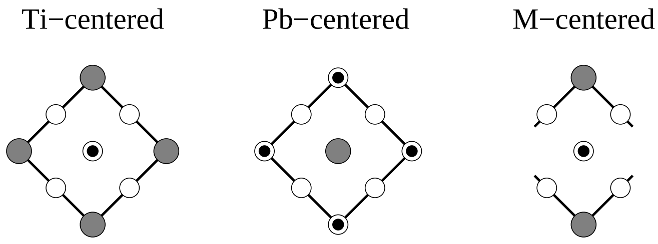

FIG. 5. Sketch of the three different choices of unit cells used for the calculation of local polarization via Born effective charges. Shown is the projection on the x–z–plane (see Fig. 1(a)).

this case, Eq. (1) simply gives the bulk macroscopic polarization. In the inhomogeneous case the spatial decomposition indicated by Eq. (1) is somewhat arbitrary, but we think that it is a rather natural choice. Of course, the cell-by-cell polarization now depends on the choice of unit cell in Fig. 5. Moreover, in principal it would be necessary to calculate the Born effective charge tensor for each atom in the neighborhood of the domain wall, since these will differ from the bulk-like values. Here, we make the further assumption of using the *cubic bulk* effective charge tensors in Eq. (1). Previous work has shown that the $\mathbf{Z}^*_\alpha$ matrix elements change by less than 10 % in going from the cubic to the tetragonal phase of $PbTiO_3$.[18] We expect a variation of similar magnitude for the atoms in the interior of the domain wall. Moreover, the sum rule for the Born effective charges guarantees that a simple uniform translation of the entire contents of the domain-wall supercell will not change the $\mathbf{P}^{(i)}$ values at all. We therefore think this is a reasonable approximation. However, it is clear that the results presented on the basis of this approximation should be regarded mainly as a visualization of the complex atomic relaxation pattern, not as a realistic calculation of the spatial polarization field. In fact, one should keep in mind that defining a local polarization is an intrinsically subtle task. The polarization is a macroscopic quantity, and there is always some ambiguity when this concept is transferred to an atomistic level.

For the Born effective charges Z^*_α we took the theoretical values for the cubic structure of $PbTiO_3$ as calculated by Zhong, King-Smith and Vanderbilt.[18] Using Eq. (1) together with the atomic displacements from Table I we get a bulk polarization of $89.5\,\mu\mathrm{C/cm^2}$. This result is only slightly larger than the value of $81.2\,\mu\mathrm{C/cm^2}$ calculated directly[24] with the Berry-phase approach.[17] All three unit cells in Fig. 5 are centered around a Pb–Ti–O plane; we therefore assign the calculated local polarizations to the corresponding Pb–Ti–O planes and plot the polarization profiles as a function of the positions of these planes.

Such a plot is shown in Fig. 6. The corresponding curves are least-square fits to functions of the form

$$P_x(x) = P_{x,0} - A\ \mathrm{sech}^2\left(\frac{x - x_0}{\xi_{\rm DW}}\right) \tag{2}$$

and

$$P_z(x) = P_{z,0}\tanh\left(\frac{x - x_0}{\xi_{\rm DW}}\right) \tag{3}$$

where $P_{x,0}$ and $P_{z,0}$ specify the polarization deep in the domain interior, and x_0 and $2\xi_{\rm DW}$ correspond to the center-position and width of the domain wall respectively. (The factor of two in $2\xi_{\rm DW}$ is a convention that is included to facilitate comparison with experimental reports that use this convention.[9,11]) Eq. (3) is the soliton solution for a domain wall in a one-dimensional fourth-order Landau-Ginzburg-type theory.[4] However, since $PbTiO_3$ is a proper ferroelectric (or improper ferroelastic), it would be more appropriate to use the result of a sixth-order Landau-Ginzburg theory.[3,31] The solution for a domain wall would then be

$$P_z(x) = P_{z,0}\,\frac{\sinh\left(\frac{x-x_0}{\xi_{\rm DW}}\right)}{\left[B + \sinh^2\left(\frac{x-x_0}{\xi_{\rm DW}}\right)\right]^{1/2}} \tag{4}$$

which is identical to Eq. (3) for B=1. Since B=1.4 has been reported for $PbTiO_4$,[9] the deviation between the two expressions is not very large.

In Fig. 6, the component of the polarization parallel to the domain wall P_z changes its sign very abruptly over a distance of less than three lattice spacings between Pb–Ti–O–type (101) planes. Furthermore, it can be seen that the results for the local polarizations $P_z^{(i)}$ do not depend strongly on the choice of unit cell. For the Ti– and Pb–centered cell they are almost indistinguishable, and for the M–centered cell the polarization changes even more rapidly. Thus, as expected, the M–centered cell gives the finest resolution for the polarization rotation in the domain wall.

From the fits to Eq. (3) we find in all three cases a domain wall position that is very nearly halfway between two Pb–Ti–O planes. Thus, from an electrostatic point of view, the domain wall can be regarded as being essentially centered on an O–O–plane. For the domain wall width we find a value of $2\xi_{\rm DW} = 5\pm0.5$ Å. This even somewhat narrower than the results of 10±3 Å and 15±3 Å suggested by recent experiment.[9,11] However, it has to be kept in mind that the experiments were done at room temperature, whereas our calculations are for zero temperature.

Figure 6 shows that the component of the polarization perpendicular to the domain wall is almost constant, showing only a small reduction as it crosses the domain wall. The local polarizations $P_x^{(i)}$ scatter a little bit more with the choice of unit cell than in the case of the parallel components $P_z^{(i)}$, and it is more difficult to obtain meaningful fits to analytic curves. (Note also that the changes of $P_x^{(i)}$ occur on a much finer scale than those of $P_z^{(i)}$.) Despite the larger variations between the fitted curves, in all three cases the minimum of $P_x^{(i)}$ lies near the same O–O plane where P_z crosses through zero. Thus, the analysis of the $P_x^{(i)}$ curves reinforces the interpretation that the domain wall is centered on an O–O atomic plane.

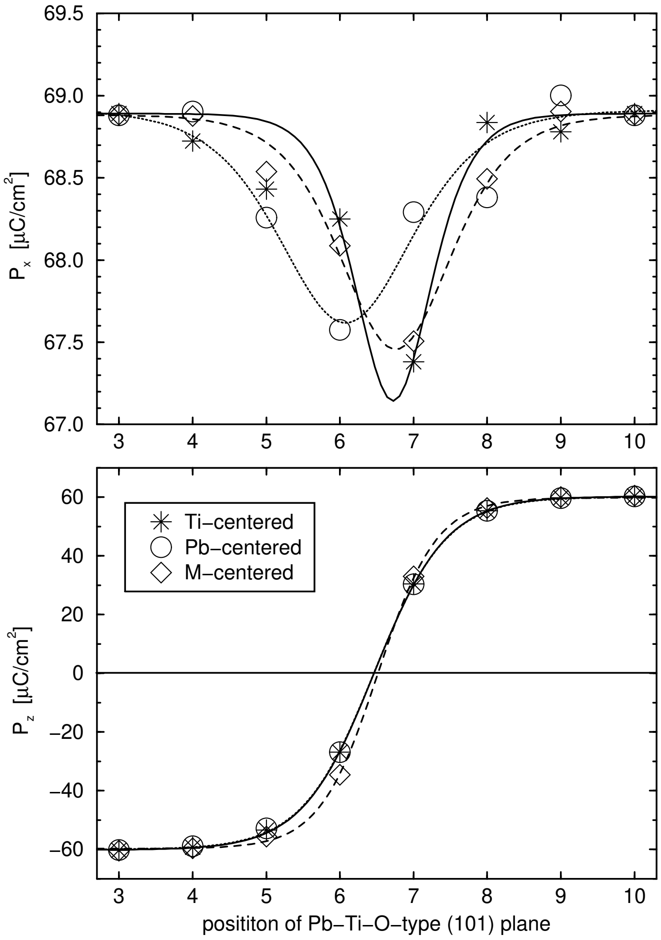

FIG. 6. Polarization profile across a 90° domain wall, calculated with a supercell of 14 perovskite unit cells. The symbols represent the local polarizations $P_x^{(i)}$ and $P_z^{(i)}$ as obtained using the three different choices of the unit cell illustrated in Fig. 5; solid, dotted and dashed lines are fits using Ti–, Pb– and M–centered unit cells, respectively.

In a full three-dimensional treatment of a Landau-Ginzburg model Cao and Cross[3] found a quasi-one-dimensional solution for the polarization profile across 90° domain walls with a constant perpendicular component $P_x(x)$. However, this analytic solution was obtained for a special choice of parameters in the Landau-Ginzburg functional, and our result of a varying $P_x(x)$ is not in contradiction with their final system of differential equations for the general case.

Finally, we note that while the reduction in $P_x^{(i)}$ in the interior of the domain wall appears rather small, it may

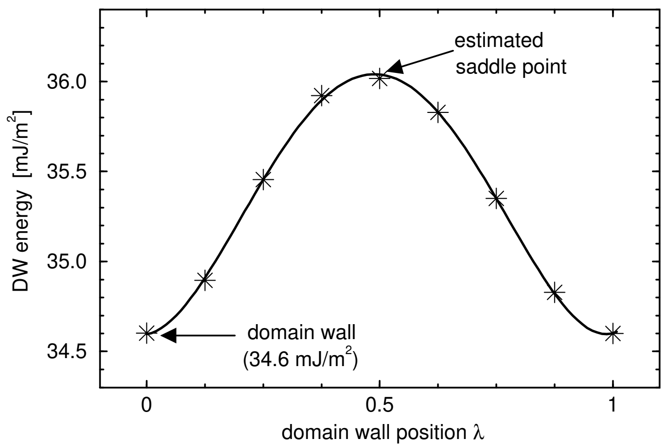

FIG. 7. Energy profile along the estimated path for the motion of a 90° domain wall, calculated with supercells of 10 perovskite unit cells.

have important consequences for the electrostatics of 90° domain walls. We return to this point in Sec. IV D.

C. Barrier for domain wall motion

As in the case of the 180° domain wall, we address here only the situation in which the entire 90° domain wall moves coherently from one (101) lattice plane to the next, preserving periodicity parallel to the wall. For the path in configuration space along which this transformation occurs, we again formed the linear interpolation $\xi_n + \lambda(\xi_{n+1} - \xi_n)$ between the atomic configurations ξ_n and ξ_{n+1} of two fully relaxed supercells with domain wall positions on nearest-neighbor (101) lattice planes.

The energies of these atomic configurations are plotted as a function of λ in Fig. 7. The energy profile is found to be a rather featureless cosine-like curve with a maximum at $\lambda \approx 0.5$. The energy at this maximum provides an estimate of the barrier height E_{barrier} for the translation of a 90° domain wall to a neighboring lattice plane. To be more precise, it gives an upper bound for the actual barrier, since our assumed path is only an approximation to the true one. To refine this estimate further, we inspected the forces remaining on the atoms at our estimated saddle-point configuration at $\lambda = 0.5$. These forces were very small, only slightly above the convergence criteria used in the structural optimization process. Following a line minimization in configuration space along the direction given by this force vector, the barrier height was lowered by less than $0.15\,\text{mJ/m}^2$.

The results for E_{barrier} obtained using various supercells are listed in Table III. At about $1.6\,\text{mJ/m}^2$, this barrier is extremely small. It is only ~4 % of the creation energy of the 90° domain wall, to be compared with the 180° case where the barrier height is ~30 % of the domain-wall energy. Or, to put it in relation to thermal fluctuations, a barrier height of $1.6\,\text{mJ/m}^2$ over the area of 12 perovskite unit cells corresponds roughly to $k_B T$ at room temperature. Therefore, as long as no pinning centers are present, the domain wall may be expected to fluctuate rather freely except at very low temperature. Clearly, it will be important to take this behavior into account when interpreting experimental probes of the widths and other properties of the 90° domain walls.

D. Electrostatic potential step across the domain wall

In Sec. II B we pointed out that the left and right sides of a 90° domain wall are not related by any symmetry operation. It follows that the charge distribution across the domain wall may have the character of a dipole layer, such that the macroscopic electrostatic potential would experience a step across the domain wall. As a general rule, if something is not prevented by symmetry, it should be present. For example, all wurzite crystals have some spontaneous polarization, since it is not prevented by symmetry; the only question is how large it may be. By the same token, since a step in the electrostatic potential is not ruled out by symmetry, it should exist for any 90° domain wall in a ferroelectric material. The issue then is to determine the sign and magnitude of such a step. Of course, it might have turned out to be insignificantly small, but we show now that this is *not* the case.

In Sec. IV B we found that the component P_x of the polarization perpendicular to the domain wall is slightly reduced in the interior of the domain wall. A decreasing (increasing) polarization on the left (right) side of the domain wall leads to an accumulation of positive (negative) charge, as is sketched in Fig. 8(a). Thus, the dip in P_x visible in Fig. 6(a) is a direct fingerprint of the existence of such a dipole layer. As a consequence, the electrostatic potential should jump from one side of the domain wall to the other, leading to band offsets for both the valence and conduction bands (see Fig. 8(b)). Mathematically, if $v(\mathbf{r})$ is the electron potential energy, Poisson's equation

$$\nabla^2 v(\mathbf{r}) = -4\pi\, e\, \text{div}\, \mathbf{P}(\mathbf{r}) \tag{5}$$

can be manipulated to the form

$$\mathrm{d}^2 \bar{v}/\mathrm{d}x^2 = -4\pi\, e\, \mathrm{d}\bar{P}_x/\mathrm{d}x \tag{6}$$

where barred quantities are y-z planar averages, e.g.,

$$\bar{v}(x) = \frac{1}{A}\int_A v(\mathbf{r})\, \mathrm{d}y\, \mathrm{d}z \quad . \tag{7}$$

Then it follows that the offset Δv in the electrostatic potential for the electrons is

$$\Delta v = -4\pi\, e \int \left(P_x(x) - P_{x,0}\right) \mathrm{d}x \quad . \tag{8}$$

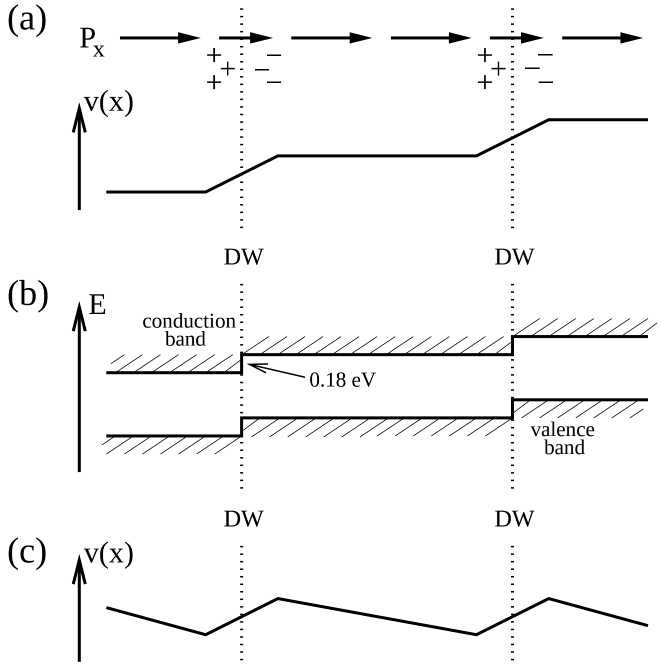

FIG. 8. Schematic illustration of a periodic array of 90° domain walls (DW's). (a) The component P_x of the polarization perpendicular to the DW, and the resulting induced charge and electron potential $v(x)$, assuming zero macroscopic electric field in the interior of each domain. (b) Corresponding band offsets. (c) Potential $v(x)$ in the case of the corresponding supercell calculation using periodic boundary conditions, i.e., in which the supercell-averaged electric field is zero.

Using the fits to Eq. 2 illustrated in Fig. 6(a), we find $\Delta v = 0.18\,\text{eV}$.

The dipole barrier can be estimated in a completely independent way by directly inspecting the electrostatic potential $v(\mathbf{r})$ that is calculated in the Kohn-Sham supercell calculation. We first compute planar averages as in Eq. (7) and then take sliding-window averages

$$\widetilde{v}(x) = \frac{1}{L}\int_{-L/2}^{L/2} \bar{v}(x')\,\mathrm{d}x' \tag{9}$$

over a window whose width is the distance L between two (101) planes. The resulting $\widetilde{v}(x)$ is shown in Fig. 9.

In order to interpret such a figure, it is important to understand the role of periodic boundary conditions in the supercell calculation. The situation sketched in Fig. 8(a) is incompatible with such boundary conditions; although the charge density is periodic, the potential is not. In all practical DFT/LDA calculations, the potential is obtained by solving Poisson's equation under periodic boundary conditions, resulting in a periodic potential as sketched in Fig. 8(c). In fact, the potentials of Fig. 8(a) and (c) differ by just a linear potential; in other words, in the latter case an artificial uniform electric field has been added in order to cancel the potential jump at the supercell boundary. Thus, instead of a step-like behavior as in Figs. 8(a), we expect a zig-zag behavior as shown in Fig. 8(c).

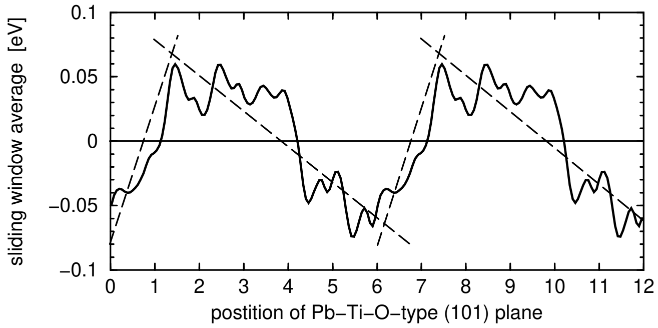

FIG. 9. Sliding-window averaged electron potential $\widetilde{v}(x)$ across the 90° domain wall, calculated with a supercell of 12 perovskite unit cells.

Despite using the sliding-window average, the electrostatic potential in Fig. 9 still contains substantial noise arising from the different atomic relaxations in the atomic planes parallel to the domain wall. Nevertheless, the expected zig-zag behavior is evident, as indicated by the dashed lines. In particular, the potential jump is very close to the expected location where P_z changes sign between two Pb–Ti–O planes (compare with Figs. 6 and 9), and the height $\Delta v = 0.16\,\text{eV}$ of the jump is in very good agreement with our previous estimate of $0.18\,\text{eV}$ based solely upon atomic positions, without any information about the electrostatic potential.

We end this section with a few remarks on the effects of the artificial electric field that is introduced in our supercell calculation by the dipole layer at the domain wall. The strength of this field depends on the supercell size and decreases only linearly with reciprocal domain-wall separation. It will therefore have some effects on the atomic relaxations. For example, if we look at the local polarization in the center of the domains, Table IV, we see that the angle α of the polarization with the x axis is not $\arctan(c/a) = 46.3°$, as would be expected for an ideally twinned crystal, but is slightly reduced. The tilt of the polarization toward the x axis can be seen to decrease with supercell size, and the angle α converges toward it ideal value. Furthermore, the amplitude of the polarization in the center of the domains is slightly larger than in the undisturbed bulk system. It is natural to interpret this excess polarization as having been induced by the artificial electric field. A rough estimate shows that for the electric field that is present, such an increase in the polarization can be expected if we assume a dielectric constant of roughly 50, which is not unreasonable. Overall, these small effects of the artificial electric field are most likely the origin of the slower convergence with supercell size of the domain-wall energy and migration barrier height compared to the 180° case, where no such electric field is present.

N	$P_{x,0}$	$P_{z,0}$	P	α
6	74.7	42.9	86.1	29.8
8	72.4	52.4	89.3	35.9
10	70.8	57.8	91.5	39.2
12	69.7	59.4	91.6	40.4
14	68.9	60.4	91.6	41.3
bulk	61.9	64.7	89.5	46.3

TABLE IV. The x and z components of the polarization (μC/cm^2) in the centers of the domains for different supercell sizes N. P is the norm of the polarization vector and α its angle with respect to the x–axis.

V. SUMMARY

In summary, we have studied the properties of 180° and 90° domain walls in $PbTiO_3$ using density-functional theory and the local-density approximation. Metastable supercells representing both kinds of domain walls were constructed, and the fully relaxed atomic configurations of the domain walls were obtained by minimizing the residual forces on the ions.

In the 180° case, the domain wall located on a Pb–O lattice plane is lowest in energy, whereas the Ti–centered wall is a saddle point configuration that spontaneously transforms into a Pb–centered wall. The domain wall is found to be very narrow, with a width on the order of the lattice constant a, and the energy to create a 180° domain wall is calculated to be 132 mJ/m^2, in very good agreement with a previous ab-initio study.

For the 90° domain wall we found a much lower domain-wall energy of 35 mJ/m^2. From the polarization profile across the domain wall we obtained the position of the wall to be halfway between Pb–Ti–O planes. We also find a domain-wall width of 5$\pm$0.5 Å, the same order of magnitude as for the 180° wall. This conclusion about the narrowness of the 90° domain wall is in line with two recent HRTEM experiments. Together, these works indicate that the conventional wisdom, which holds that the 90° domain wall is much broader than its 180° counterpart, does not hold true in $PbTiO_3$.

On the other hand, the barrier height for the coherent motion of a 90° domain wall to a neighboring lattice plane is estimated to be very small. The domain wall can easily move so that a scenario where the domain wall is pinned at defects and fluctuates widely in between is very likely to occur in real samples. The apparent width of the domain boundary may therefore be much broader, raising the question as to what exactly we mean by the "width of a domain wall." In this regard, our result $2\xi_{\rm DW} = 5\pm0.5$ Å for an ideal, defect-free wall should be regarded as a intrinsic width of the domain boundary at zero temperature, whereas at finite temperatures the domain wall may be smeared out by fluctuations. Regarding the sharp HRTEM images of the 90° domain walls, we also have to take into account that the samples in these kinds of experiments are very thin (typically 10 nm) so that surface pinning of the domain walls could play an important role.

Finally, we have found an electrostatic dipole moment across the 90° domain wall, which causes a step in the electrostatic potential and an offset of the valence and conduction bands of 0.15–0.2 eV. To our knowledge, the existence of such a dipole moment across a ferroelectric domain wall has never been reported in literature before. It remains a challenge whether such an effect can be observed experimentally.

VI. ACKNOWLEDGMENTS

We wish to thank Jim Scott and Sami Pöykkö for useful discussions. This work is supported by the ONR grant N00014-97-1-0048.

[1] V.A. Zhirnov, Sov. Phys. JETP **35**, 822 (1952).
[2] L.N. Bulaevskii, Sov. Phys. Solid State **5**, 2329 (1960).
[3] W. Cao, G.R. Barsch, J.A. Krumhansl, Phys. Rev. B **42**, 6396 (1990); W. Cao, L.E. Cross, Phys. Rev. B **44**, 5 (1991).
[4] M.E. Lines and A.M. Glass, *Principles and Applications of Ferroelectrics and Related Materials*, Clarendon Press, Oxford, 1977.
[5] J. Padilla, W. Zhong, and D. Vanderbilt, Phys. Rev. B **53**, R5969 (1996).
[6] S. Pöykkö and D.J. Chadi, Appl. Phys. Lett. bf 75, 2830 (1999); J. Phys. and Chem. of Solids **61**, 291 (2000).
[7] A.L. Bursill and P.J. Lin, Ferroelectrics **97**, 71 (1986).
[8] F. Tsai, V. Khiznichenko, and J.M. Cowley, Ultramicroscopy **45**, 55 (1992).
[9] S. Stemmer, S.K. Streiffer, F. Ernst, and M. Rühle, Phil. Mag. A **71**, 713 (1995).
[10] N. Floquet, C.M. Valot, M.T. Mesnier, J.C. Niepce, L. Normand, A. Thorel, and R. Kilaas, J. Phys. III France **7**, 1105 (1997); N. Floquet and C. Valot, Ferroelectrics **234**, 107 (1999).
[11] M. Foeth, A. Sfera, P. Stadelmann, and P.-A. Buffat, J. of Electron Microscopy **48**, 717 (1999).
[12] P. Hohenberg and W. Kohn, Phys. Rev. **136**, B864 (1964); W. Kohn and L.J. Sham, Phys. Rev. **140**, A1133 (1965).
[13] D.M. Ceperley and B.J. Alder, Phys. Rev. Lett. **45**, 566 (1980); J.P. Perdew and A. Zunger, Phys. Rev. B **23**, 5048 (1981).
[14] R.E. Cohen and H. Krakauer, Phys. Rev. B **42**, 6416 (1990); R.E. Cohen, Nature **358**, 136 (1992).
[15] R.D. King-Smith and D. Vanderbilt, Phys. Rev. B **49**, 5828 (1994).
[16] W. Zhong, D. Vanderbilt, and K.M. Rabe, Phys. Rev. Lett. **73**, 1861 (1994); Phys. Rev. B **52**, 6301 (1995).

[17] R.D. King-Smith and D. Vanderbilt, Phys. Rev. B **47**, 1651 (1993).
[18] W. Zhong, R.D. King-Smith, and D. Vanderbilt, Phys. Rev. Lett. **72**, 3618 (1994).
[19] Ph. Ghosez, J.-P. Michenaud, and X. Gonze, Phys. Rev. B **58**, 6224 (1998).
[20] G. Sághi-Szabó, R.E. Cohen, and H. Krakauer, Phys. Rev. Lett. **80**, 4321 (1998); H. Fu and R.E. Cohen, Nature **403**, 281 (2000).
[21] Ph. Ghosez, E. Cockayne, U.V. Waghmare, and K.M. Rabe, Phys. Rev. B **60**, 836 (1999).
[22] C.H. Park and D.J. Chadi, Phys. Rev. B **57**, 13961 (1998); S. Pöykkö and D.J. Chadi, Phys. Rev. Lett. **83**, 1231 (1999).
[23] R.E. Cohen, J. Phys. Chem. Solids **57**, 1393 (1996); J. Padilla and D. Vanderbilt, Phys. Rev. B **56**, 1625 (1997).
[24] B. Meyer, J. Padilla, and D. Vanderbilt, Faraday Discuss. **114**, 395 (1999); B. Meyer and D. Vanderbilt, Phys. Rev. B **63**, 205426 (2001).
[25] D. Vanderbilt, Phys. Rev. B **41**, 7892 (1990).
[26] F. Jona, G. Shirane, *Ferroelectric Crystals*, Dover, New York, 1993.
[27] W.H. Press, S.A. Teukolsky, W.T. Vetterling, B.P. Flannery, *Numerical Recipes*, Cambridge University Press, New York 1986.
[28] H.J. Monkhorst and J.D. Pack, Phys. Rev. B **53**, 5188 (1976).
[29] Y.G. Wang, J. Dec, and W. Kleemann, J. Appl. Phys. **84**, 6795 (1998).
[30] J. Moreno, J.M Soler, Phys. Rev. B **45**, 13891 (1992).
[31] G.R. Barsch, J.A. Krumhansl, Phys. Rev. Lett. **53**, 1069 (1984).